Pattern formation in oscillatory media without lateral inhibition

Rehman Ali, Jeremy Harris, and Bard Ermentrout

Phys. Rev. E **94**, 012412 — Published 29 July 2016

DOI: 10.1103/PhysRevE.94.012412

Pattern Formation in Oscillatory Media without Lateral Inhibition

Rehman Ali*
Department of Biomedical Engineering, Georgia Institute of Technology

Jeremy Harris * and Bard Ermentrout
Department of Mathematics, University of Pittsburgh
(Dated: July 1, 2016)

Spontaneous symmetry breaking instabilities are the most common mechanism for how biological, chemical, and physical systems produce spatial patterns. Beginning with Turing's original paper, so-called lateral inhibition—in which negative feedback has greater spread than positive feedback—has been the underlying mechanism for pattern formation in biological models. Despite this, there are many biological systems that exhibit pattern formation but do not have lateral inhibition. In this paper, we present an example of such a system that is able to generate robust patterns emerging from a spatially homogeneous state. In fact, patterns can arise when there is *only* spatial spread of the activator. Unlike classic Turing pattern formation, these patterns arise from a spatially homogeneous oscillation rather than from a constant steady state.

PACS numbers: 05.45.Xt,87.19.lm,87.18.Cf

I. INTRODUCTION

Spontaneous symmetry breaking from a spatially uniform state is the most common mechanism for pattern formation in many physical systems [1, 2]. Typically, one starts with a spatially uniform constant solution and then performs a linear stability analysis to determine when there will be instability. Depending on the modes that become unstable, complex spatio-temporal patterns arise that include hexagons, stripes, of various orientations, and more complicated temporally varying patterns [2, 3]. In a biological or chemical setting, models for pattern formation begin with two species: an activator and inhibitor (or, excitatory and inhibitory components), and in order to get pattern formation, assume that the reach of the inhibitor is greater than that of the activator (so-called *lateral inhibition*). However, there are many systems where the negative (inhibitory) feedback does not spatially extend beyond the positive (activator) feedback. Furthermore, it may be that the spatially uniform state is not constant, but rather is oscillatory. Thus, it is of general interest to see whether or not lateral inhibition is necessary to get pattern formation in any homogeneous system and if not, how such patterns might arise.

In the nervous system, symmetry-breaking patterns have been associated with visual hallucinations, working memory, and feature maps. In each of the models that leads to pattern formation, there is an explicit assumption that the spatial spread of inhibition extends farther than that of excitation. However, it has been shown in certain areas of sensory cortex that inhibition has slightly less or about the same spread as excitation. For instance, Levy and Reyes present distance-dependent connection profiles for data from primary auditory cortex in mouse and show that for two broad classes of interneurons, fast-spiking and non-fast-spiking cells, the synaptic connection profiles for inhibition to excitation is narrower than the reciprocal (excitation to inhibition) connection profile [4]. In this paper, we show that a spatially extended two population model of cortex can exhibit spatio-temporal patterns without assuming lateral inhibition. We show that for some choices of parameters, it is possible to get symmetry breaking instabilities even when there is *no spread of inhibition*, that is when inhibition is only local.

II. A WILSON-COWAN NETWORK WITH SPATIAL COUPLING

We begin with the classical Wilson-Cowan equations (WC) in which there is a population of excitatory neurons connected to another population of inhibitory neurons:

$$\tau_e \frac{\partial u}{\partial t} = -u + F(a_{ee}K_e(x) \star u - a_{ei}K_i(x) \star v - \theta_e) \quad (1)$$
$$\tau_i \frac{\partial v}{\partial t} = -v + F(a_{ie}K_e(x) \star u - a_{ii}K_i(x) \star v - \theta_i)$$

where u, v are the activities of the excitatory and inhibitory populations, respectively; the parameters τ_j, $j \in \{e, i\}$ represent the time scales of the excitatory and inhibitory activities; the parameters $a_{j\,k}$ are the coupling strengths from population k to population j and θ_j are thresholds; and $F(I)$ is a nonlinear function representing the firing rate as a function of the spatially distributed inputs: $K_j(x)$, $j \in \{e, i\}$ are spatial interaction functions (typically Gaussian or exponentially decaying with Euclidean distance) which are convolved with the activities. In general, $K_j(x) = K(x/\sigma_j)/\sigma_j$ where σ_j is the characteristic spatial length. If $\sigma_i > \sigma_e$, we have the classic version of pattern formation *with* lateral inhibition, since the length scale of inhibition exceeds that of excitation. In this manuscript, we show results for the exponential

* These authors contributed equally to the manuscript.

kernel that decays with distance, which for the 1D spatial model is given by

$$K_j(|x|) = \frac{1}{2\,\sigma_j}\,\exp\left(-\frac{|x|}{\sigma_j}\right) \quad , \quad j \in \{e,\, i\}\ .$$

Throughout this paper, we let $F(I) = 1/(1+\exp(-\beta\, I))$ and $\beta = 50, a_{ee} = a_{ie} = 1, a_{ei} = 1.5, a_{ii} = 0.25$, $\theta_i = 0.4$. The remaining parameter θ_e and the relative time and space constants, defined as $\tau = \tau_i/\tau_e$ and $\sigma = \sigma_i/\sigma_e$, respectively, will be varied.

III. THE SPATIALLY HOMOGENEOUS SYSTEM

In the absence of spatial connectivity, the system in Eq. (1) simplifies to a planar system of differential equations given by

$$\begin{aligned} \tau_e \frac{du}{dt} &= -u + F(a_{ee}u - a_{ei}\,v - \theta_e) \qquad (2)\\ \tau_i \frac{dv}{dt} &= -v + F(a_{ie}\,u - a_{ii}\,v - \theta_i)\ . \end{aligned}$$

Note that solutions of Eq. (2) are solutions of the partial integro-differential equation given in Eq. (1) as long as the spatial kernels, $K_e(x)$ and $K_i(x)$, are normalized.

In Figure 1, we show the phase planes and bifurcation diagrams for the system in Eq.(2), corresponding to two different values of the threshold parameter, $\theta_e = 0.125$ and $\theta_e = 0.08$. For all values θ_e of interest, there is an up-state equilibrium, $E := (u_m, v_m)$, that occurs at the region of the u-nullcline where the slope is positive. Presumed to be the active state of the visual cortex, Ozeki et al. call this the inhibitory-stabilized network (ISN) state [5]. Depending on the time scale $\tau = \tau_i/\tau_e$, the equilibrium point E is either a stable or an unstable node. The bifurcation diagram as τ varies is shown in Fig. 1(c) for $\theta_e = 0.125$. At low values of τ, E is stable, and as τ increases, it loses stability through a Hopf bifurcation; a branch of stable periodic orbits emerges from the Hopf bifurcation, and the green curve in Fig. 1(a) is one such periodic orbit. Finally, as τ further increases, the curve of periodic orbits terminates at a homoclinic bifurcation. This is shown with a blue dot in Fig. 1(c), and the corresponding homoclinic orbit is the larger of the two closed curves in Fig. 1(a). For θ_e small enough, E is the only equilibrium, and if τ is small enough, it is stable; otherwise, there is a stable limit cycle, as in Fig. 1(b). In panel (d), we show that the green curve of limit cycles persist for all $\tau > \tau_{HB}$ when $\theta_e = 0.08$.

For the spatially extended WC system, symmetry-breaking pattern formation can occur at the spatially homogeneous equilibrium, E, when there is lateral-inhibition ($\sigma_i > \sigma_e$) and τ is small enough so that there are no limit cycles in the homogeneous system [6]. Figure 2(a) depicts such a case in which we observe spatially periodic, time-invariant stripes. While it is possible to obtain pattern formation from a homogeneous equilibrium in the WC equations when $\sigma_e \lesssim \sigma_i$, the conditions require careful tuning of parameters and the difference between the two length scales is small (see appendix for calculations). However, since in most cortical circuits, the spatial extent of inhibition is generally less than that of excitation, we now let $\sigma_i = 6.67 < 10 = \sigma_e$, and increase $\tau = 0.4$ so that there is a bulk oscillation, i.e. a spatially homogeneous, temporally periodic solution, as shown in Fig. 2(b). Further increasing $\tau = 0.6$ causes the spatially homogeneous oscillation to become unstable, which results in a pattern that is periodic in both space and time, as shown in Fig. 2(c).

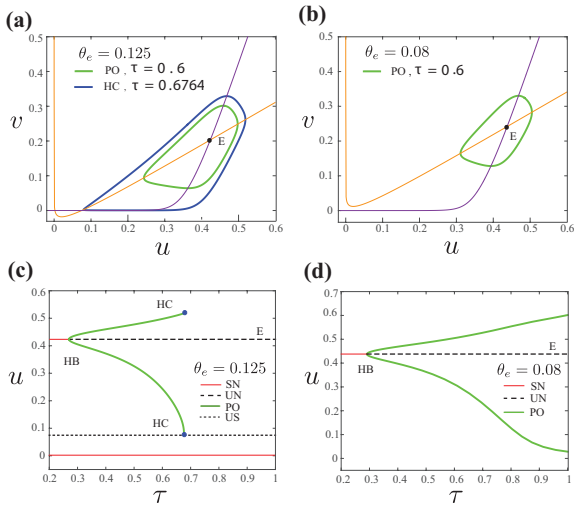

FIG. 1. Phaseplane and bifurcation diagram of the ISN state. (a) Phaseplane for $\theta_e = 0.125$ with periodic orbit (PO), $\tau = 0.6$, and homoclinic (HC), $\tau = 0.6764$; (b) Phaseplane for $\theta_e = 0.08$. with PO, $\tau = 0.6$. (c) Bifurcation as τ increases when $\theta_e = 0.125$, showing three equilibria: Stable node, SN; unstable saddle, US; unstable node, UN; equilibrium point E. Stable PO's grow from a Hopf bifurcation (HB) of the upper equilibrium E and terminate at a homoclinic, HC; (d) Same as (c) but for $\theta_e = 0.08$ to show the PO's exist for all $\tau > \tau_{HB}$.

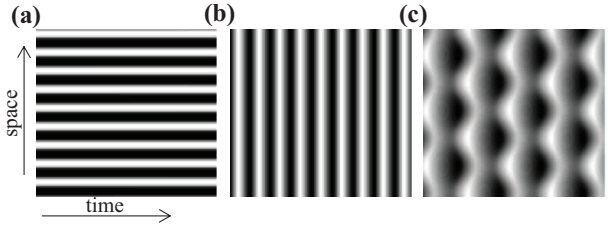

FIG. 2. Simulations for a network ($n = 256$) of coupled WC-type neurons. (a) Classic Turing patterns from a steady state when $\theta_e = 0.08$, $\sigma_e = 10$, $\sigma_i = 20$, and $\tau = 0.2$. (b) Reducing σ_i to 6.67 and increasing $\tau = 0.4$ induces a spatially homogeneous periodic oscillation. (c) Further increasing $\tau = 0.6$ results in periodic spatiotemporal patterns.

IV. LINEAR STABILITY OF THE SPATIALLY HOMOGENEOUS OSCILLATION

In order to investigate the bifurcation from a homogeneous constant state, we simply linearize and take the Fourier transform resulting in a family of 2×2 matrices whose eigenvalues are easy to compute (see appendix). However, in the present case (e.g. as in Fig. 2(b),(c)), the spatially homogeneous solution is a periodic orbit, so we must take a different approach. We linearize Eq. (1) around the spatially homogeneous periodic solution, $(\bar{u}(t), \bar{v}(t))$, and perturb the solution with respect to spatial frequency ω. We take the perturbation to be of the form

$$U(x,t) = \bar{u}(t) + \varepsilon\, u(t)\, e^{i\,\omega\, x} \quad , \quad V(x,t) = \bar{v}(t) + \varepsilon\, v(t)\, e^{i\,\omega\, x} \, ,$$

so that

$$\begin{aligned} K_e \star U(x,t) &= \bar{u}(t) + \varepsilon\, \hat{K}_e(\omega)\, u(t)\, e^{i\omega\, x} \\ K_i \star V(x,t) &= \bar{v}(t) + \varepsilon\, \hat{K}_i(\omega)\, v(t)\, e^{i\omega\, x} \, , \end{aligned} \tag{3}$$

where $\hat{K}_j(\omega)$ are the Fourier transforms of $K_j(x)$. After a Taylor expansion and collecting order ε terms, we obtain a family of linear two-dimensional equations, parameterized by wavenumber, ω:

$$\begin{aligned} u_t &= -u + b_{ee}(t)\hat{K}_e(\omega)u - b_{ei}(t)\hat{K}_i(\omega)v \\ \tau v_t &= -v + b_{ie}(t)\hat{K}_e(\omega)u - b_{ii}(t)\hat{K}_i(\omega)v \, , \end{aligned} \tag{4}$$

where $b_{jk}(t) = a_{jk}\, F'(a_{j,e}\, \bar{u}(t) - a_{j,i}\, \bar{v}(t) - \theta_j)$ and where $\tau = \tau_i/\tau_e$ is the time constant of inhibition relative to excitation. If the homogeneous state of the system is an equilibrium point, then b_{jk} are just constants and the stability reduces to the usual Turing-type analysis for constant steady states [7]. If, on the other hand, the homogeneous solutions are oscillatory (as will be the case for $\tau > \tau_{HB}$), then Equation (4) is a linear periodic system which we can write as $X' = A(t;\omega)X$ with

$$A(t;\omega) = \begin{pmatrix} -1 + b_{ee}(t)\hat{K}_e(\omega) & -b_{ei}(t)\hat{K}_i(\omega) \\ \left(b_{ie}(t)\hat{K}_e(\omega)\right)/\tau & \left(-1 - b_{ii}(t)\hat{K}_i(\omega)\right)/\tau \end{pmatrix} .$$

Here we include the parameter ω to emphasize that the solutions depend on the wavenumber perturbation. We solve this linear T-periodic equation with initial conditions, $X = I$, where I is the identity matrix, to form a principal matrix of solutions. After one period, we obtain the Monodromy matrix $M(\omega) := X(T;\omega)$ which, for our system, is a 2×2 matrix, parametrized by ω. If any of the eigenvalues of $M(\omega)$ have magnitude greater than 1 for some value of ω, then the limit cycle will lose stability with spatial mode ω. With a 2×2 matrix M, there are three ways to lose stability: (i) a real eigenvalue increases above 1; (ii) a real eigenvalue decreases below -1; (iii) a complex pair obtains a magnitude greater than 1.

One need only check the determinant (D) and the trace (Tr) of $M(\omega)$ to test these conditions: (i) $Q_1 := 1 - Tr + D > 0$; (ii) $Q_2 := 1 + Tr + D > 0$; (iii) $Q_3 := 1 - D > 0$. That is, if any of these test functions falls below 0 as some parameter such as ω changes, then an instability will occur. Figure 3 shows a schematic of these conditions.

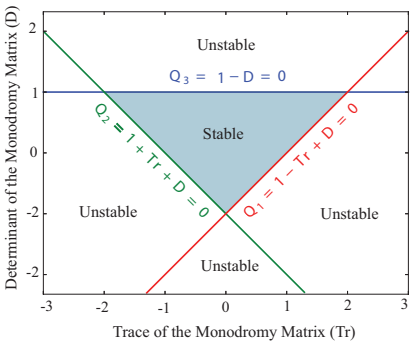

FIG. 3. Diagram to show the boundaries for instability in terms of the trace (Tr) and determinant (D) of the Monodromy matrix.

With this background, we numerically solve the spatially homogeneous equations for one period, compute the Monodromy matrix, and then look for zero crossings of the three quantities. We have found that only Q_2 changes sign as ω varies, so henceforth, this is the only test function that we follow. We note that Q_2 signifies a period-doubling bifurcation, so we expect the bifurcatiing solution to repeat every other cycle, such as the pattern shown in Fig. 2(c).

There are three parameters of interest to us: (1) The inhibitory space constant σ_i, (2) the inhibitory time constant τ_i, and (3) the excitatory threshold θ_e. Since space and time can be rescaled, the inhibitory space and time constants in Figures 4-7 are relative to those of excitation: $\tau = \tau_i/\tau_e$ and $\sigma = \sigma_i/\sigma_e$. The excitatory threshold, θ_e, switches the system from one to three equilibria and determines if the limit cycles terminate on a homoclinic orbit (see Fig. 1(a)). We find that for large enough space constant σ, the quantity $Q_2(\omega)$ has two roots that signify an interval of wavenumbers, ω, for which the homogeneous limit cycle is unstable. In Fig. 4, the blue curves show the graph of Q_2 as a function of wave number ω for a fixed value of σ. By varying σ, we can cause the two roots, indicated by the green curve in Fig. 4, to come together at a double root. This corresponds to a turning point of the green curve in the (σ, ω) plane, as seen in the right panel. The critical value of σ at which this occurs sets the boundary for pattern forming instabilities.

From here, we can follow the critical value of σ as τ varies for different choices of θ_e to obtain a family of curves that delineate where the homogeneous limit cycle is unstable. In Figure 5, we show these curves for the exponential kernel and find several qualitatively different aspects of them. Consider when $\theta_e = 0.125$, large enough so that there are three equilibria. In this case, limit cycles exist for τ-values between the Hopf and the homoclinic ($\tau_{HC} \approx 0.67$, for $\theta = 0.125$) bifurcations, and

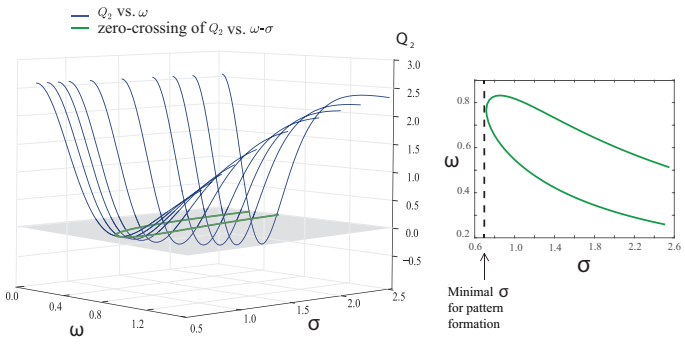

FIG. 4. Surface plot of the test function Q_2 as a function of (σ, ω) for $\theta_e = 0.08$ and $\tau = .5$. Each blue curve is Q_2 as a function of ω for fixed σ. The green curve indicates the level set $Q_2 \equiv 0$ as σ and ω vary, and the right panel depicts the green curve in the gray plane. As σ decreases, the two zeros come together at the turning point of the green curve; this sets the minimal σ for pattern formation, which in this case is $\sigma \approx .716$, indicated by the vertical dashed line.

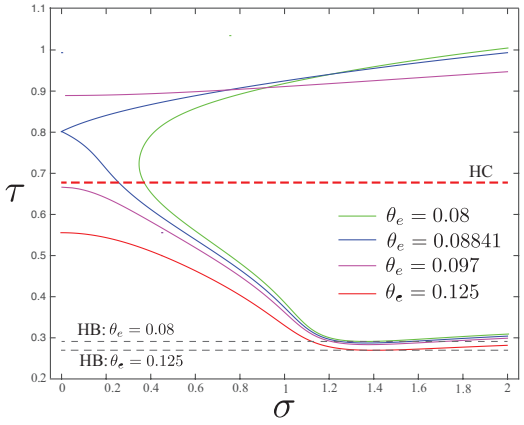

FIG. 5. Stability diagram for the homogeneous periodic orbit as the parameters (σ) and time constant (τ) vary for the spatially extended WC model. The homoclinic (HC) line corresponds to $\theta_e = 0.125$. Hopf bifurcations occur at the minima of each of the lower plotted curves.

the instabilities occur between the solid and dashed (red) curves. The Hopf bifurcations (independent of σ) occur at the values of τ that are minima for the lower pattern forming cuves. When $\theta_e < 0.09783$,(the value for a saddle-node of equilibria), e.g. $\theta_e = 0.08$, there is a unique equilibrium point and a spatially homogeneous limit cycle for all $\tau > \tau_{HB}$. That is, there is no homoclinic boundary. In this case, there is a turning point in the stability curve which bounds the minimal value of σ for pattern formation away from zero (shown by the three upper solid curves). In Fig. 5, we show the stability curves for several values of excitatory threshold where there is no homoclinic: for $\theta_e = 0.097$ (violet), the system is near the saddle node bifurcation of equilibria, and for $\theta = 0.08841$ (blue), there is a cusp at $\sigma = 0$. Here, we emphasize that σ can extend all the way down to $\sigma = 0$ for some choices of θ_e, so that patterns may occur even when there is only local inhibition when $\theta_e \in (0.08841, 0.09783)$.

From the stability boundaries shown in Fig. 5, it is clear, that there are regions where $\sigma < 1$ and the homogeneous state loses stability. What is more interesting is that there is an upper bound on τ for which the uniform state loses stability, which is to say that inhibition can neither be too slow nor too fast. For θ_e-values that yield a turning point in the curve (e.g. $\theta_e = 0.08$), the upper boundary increases with increasing σ. As σ passes through one, the excitatory and inhibitory populations have identical spatial scales. Moreover, the upper boundary occurs at a value of $\tau < 1$, so the symmetry-breaking mechanism relies on the difference in time scales. As we further increase the spatial scale so that $\sigma > 1$, the upper boundary passes through $\tau = 1$ and there can occur patterns when the time scales of excitatory and inhibitory populations are the same.

Next we compare the behavior of the theoretical stability curves with the behavior of the 1D spatial model. We discretize Eq. (1) into 256 points for each population, start close to the equilibrium point (with some added heterogeneity to break the symmetry) and then integrate over a range of parameters. We track the *spatial* variance of the simulation in order to automatically determine the strength of the pattern.

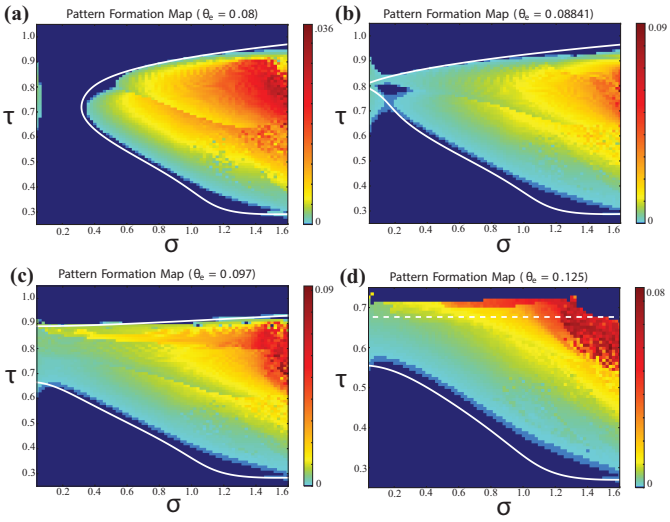

FIG. 6. Comparison between the stability diagram from the linear theory and the full simulations. (a) $\theta_e = 0.08$: Patterns remain entirely in the stability region. (b) $\theta_e = 0.08841$: When the boundary breaks open at $\sigma = 0$. (c) $\theta = 0.97$ slightly less than the value of the saddle-node bifurcation. (d) $\theta_e = 0.125$: The upper boundary (horizontal, dashed line at $\tau = 0.6764$) is the homoclinic, and patterns can exist in regions where there is no limit cycle (above the line).

Figure 6(a) shows the case of a single equilibrium point ($\theta_e = 0.08$) in which patterns seem to exist only in regions of parameter space where the uniform oscillation is unstable to spatial perturbations. Again, we remark

that if τ is too large, then the uniform oscillation is always stable for $\sigma < 1$. Fig. 6(d) shows that the bottom boundary is limiting for patterns but the top boundary (determined by the homoclinic bifurcation of the homogeneous state) is not the limiting boundary. This means that there are patterns for parameter regimes in which there is *no homogeneous limit cycle*. There is no *a priori* reason that we would expect the linear stability analysis to predict the regime of nonlinear pattern formation; it is just a condition for the uniform state to be unstable.

V. PATTERN FORMATION WITH NO SPATIAL SPREAD OF INHIBITION

Looking at Figures 6(c) and (d), there appear to be regions where there are patterns in the case of $\sigma = 0$, which is very surprising since there is now only one length scale in the system. Since this phenomena seems to depend on θ_e, we consider the behavior when $\sigma = 0$ and vary τ and θ_e. In the appendix, we show that no pattern formation can arise from a constant state when $\sigma_i = 0$ (that is, $\sigma = \sigma_i/\sigma_e = 0$). Figure 7 shows the regime in (θ_e, τ) where there exist oscillations to the uncoupled system (the bulk oscillation). For θ_e to the left of the saddle-node value, $\theta_{SN} \approx 0.09783$ (labeled SNIC in Fig. 7), there is only one equilibrium point and it is unstable for τ above the curve of Hopf bifurcations. For $\theta_e > \theta_{SN}$, the bulk oscillation exists for τ between the Hopf bifurcation curve and the lower section of the homoclinic curve. Furthermore, within the region where there is a bulk oscillation, there is a curve labeled PF, above which the bulk oscillation is unstable and we expect pattern formation. Interestingly, this region extends slightly below θ_{SN} for a limited band of τ where there is only a limit cycle and a single equilibrium point. The smallest θ_e such that there is a range of τ-values for which the bulk oscillation is unstable is approximately $\theta_e \approx 0.08841$ and corresponds to the cusp seen in figure 5 at $\sigma = 0$.

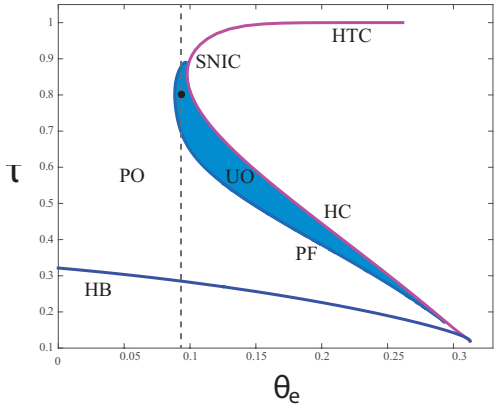

FIG. 7. Phase-diagram showing regions where there is a periodic orbit (PO) and pattern forming instabilities as τ and θ_e vary with no spread of inhibition ($\sigma = 0$). The shaded region labeled UO, bounded between the homoclinic (HC) and pattern forming (PF) curves, indicates instabilities to the bulk oscillation when $\sigma = 0$. The upper branch labeled HTC is the curve of heteroclinic orbits (joining the saddle point with the down-state), while the lower branch labeled HC is the curve of homoclinics. These come together at a turning point, corresponding to a saddle node on an invariant circle (SNIC). The vertical dashed line is $\theta_e = 0.094$, showing an interval of τ-values that give rise to pattern formation when there is one equilibrium. The black dot at $(\theta_e, \tau) = (0.094, 0.8)$ corresponds to parameters in Fig. 8(c).

VI. THE TWO-DIMENSIONAL NETWORK

Thus far, we have only considered the Wilson-Cowan equations with 1D spatial coupling and analyzed the stability of the bulk oscillation to certain wavenumber perturbations. However, the analysis for the 2D system will be identical to that of the 1D system, and in fact, it is the same for n-dimensional systems, as long as the spatial coupling profile decays with the Euclidean distance. Here we take the kernel to be the decaying exponential,

$$K_j(\sqrt{x^2+y^2}) = \frac{1}{2\,\pi\,\sigma_j^2}\,\exp\left(-\frac{\sqrt{x^2+y^2}}{\sigma_j}\right) \quad , \quad j \in \{e,\, i\}\,.$$

Then we can use the curves in Figures 5 and 6 to find parameters where we would expect patterns in the 2D spatially connected network, though the analysis will indicate nothing about the stability of the pattern itself.

To illustrate the geometry of the period-doubled branch of solutions, we create an array of 256 by 256 excitatory and inhibitory neurons with periodic boundary conditions and simulate the 2D spatially connected network. We present the spatio-temporal patterns in Fig. 8 as a series of five frames over equal time intervals for one period, T, of the period-doubled oscillation. To simulate perturbing from the spatially uniform oscillation, we impart small random fluctuations to initial conditions near the periodic orbit. When the uniform oscillation is unstable, the system may tend to the sorts of spatio-temporal patterns shown in Fig. 8, in which spatially-alternating active and quiescent states in the first column frames switch positions at half a cycle (not shown) between the third and fourth column frames.

In Figure 8(a), we let $\theta_e = 0.125$ and the rest of the parameters be the same as in Fig. 2(c) to show pattern-formation in the presence of a down-state. Then in Fig. 8(b), we increase τ to 0.7, which is above the homoclinic bifurcation indicated in Fig. 5. Here we remark that the linear stability indicates pattern formation for the parameter set in Fig. 8(a), since the point (σ, τ) falls well between the lower stability curve and the upper homoclinic boundary of Fig. 5. However, for the parameter set in Fig. 8(b), there is *no uniform state oscillation*, yet a pattern emerges. Similar to the reduced model in Fig. 9(b), the period-doubled oscillations seem to be stable

even past the homoclinic bifurcation at $\tau_{HC} = 0.6764$. Lastly, Fig. 8(c) shows pattern formation in the case when there is only local inhibition, i.e. $\sigma_i = 0$, and the parameters $(\theta_e, \tau) = (0.094, 0.8)$ correspond to the point on the vertical line within the shaded area of Fig. 7.

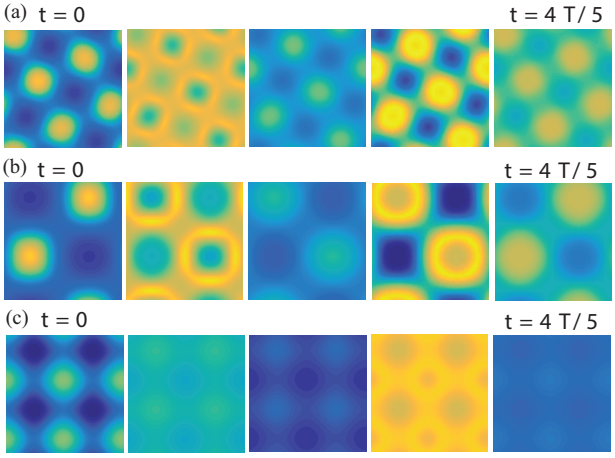

FIG. 8. Five frames over one period for simulations of the 2D Wilson Cowan model with N=256 x 256 neurons. Spatio-temporal patterns when $\sigma_e = 10$ and parameters: (a) $\sigma_i = 6.67$, $\theta_e = 0.125$, $\tau = 0.6$, $T = 11.3$; (b) $\sigma_i = 6.67$, $\theta_e = 0.125$, $\tau = 0.7$, $T = 24.5$; (c) $\sigma_i = 0$, $\theta_e = 0.094$, $\tau = 0.8$, $T = 30.1$. These parameters correspond to the black dot at $(\theta_e, \tau) = (0.094, 0.8)$ in Fig. 7. See [8] for the corresponding movies.

VII. A REDUCED MODEL

We now describe a simple, highly reduced model that helps explain the difference in behavior between Fig. 6(a) and Fig. 6(d). We create a network of two pairs, $u_{1,2}$, $v_{1,2}$, with coupling between them. The coupling of pair 2 to pair 1 has the form $(1-q_e)u_1+q_e u_2$ and $(1-q_i)v_1+q_i v_2$, with a similar coupling for pair 1 to pair 2. That is, the coupling kernels, K_e, K_i are replaced with their two-point discrete analogs. If $q_{e,i} = 0$, then there is no coupling, and if $q_{e,i} = 0.5$, then the coupling is essentially all-all. We choose $q_e = 0.166$ and $q_i = 0.05$ so that the inhibitory coupling "spread" is less than a third of the excitatory. In Figure 9, we show the two bifurcation diagrams for the reduced system where respectively $\theta_e = 0.08$ and $\theta_e = 0.125$: In panel (a) where there is only one equilibrium point and the homogenous limit cycle exists for all $\tau > \tau_{HB}$, we see the periodic orbit becomes unstable at a period doubling bifurcation, and as τ further increases, the stable branch of period-doubled orbits connects back to the periodic orbit. This is qualitatively the same picture as Fig. 6a. In contrast, panel (b) shows that while the periodic orbit becomes unstable at a period-doubling bifurcation as in (a), it does does not connect back to the branch of periodic orbits; instead, the stable period-doubled branch continues past the homoclinic bifurcation of the unstable periodic branch just as in Fig. 6d.

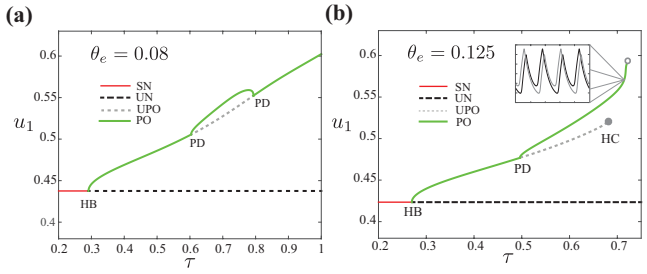

FIG. 9. Bifurcation diagram for the pair of coupled WC equations. Labeling is the same as in Fig. 1 with an additional label for the unstable periodic orbits (UPO). (a) For $\theta_e = 0.08$, the curve of period-doubled orbits connects back to the branch of unstable periodic orbits, stabilizing the homogeneous periodic solution for all τ beyond the second PD-point. (b) For $\theta_e = 0.125$, unstable periodic orbits terminate at a homoclinic, HC. The inset shows u_1 and u_2 over two periods for $\tau = 0.7 > \tau_{HC}$.

VIII. DISCUSSION

In this paper, we have shown that if the homogeneous state is a periodic solution rather than an equilibrium point, then it is quite easy to obtain pattern formation even when the inhibition has a much smaller spread than the excitation. In fact, the variance maps in Fig. 6(c) and (d) compared with the analytic curves from Figures 5 and 9 show that when τ is close to the homoclinic bifurcation, then there can be spontaneous pattern formation even if there is *no* inhibitory spread. A similar surprising result is that there can be patterns even when the excitatory and inhibitory interactions are identical; in both instances, there is only one characteristic length scale. In these cases, we observe from Fig. 5 that whenever $\sigma < 1$, the regions of instability lie below the line $\tau = 1$. This suggests that the symmetry-breaking mechanism must result from the difference in time scales of excitatory and inhibitory populations. Indeed, if the time scales and the space scales are the same, then we conjecture that no patterns can spontaneously arise from the oscillatory state.

Though we have found some similar work on pattern formation in the literature, there are notable differences between these results and results presented in this paper. For instance, Kuramoto [9] has shown the existence of complex spatio-temporal patterns. He derives an equation for the spatial phase gradient that has the form $\theta_t = a\theta_x^2 - b\,\theta_{xx} - c\,\theta_{xxxx}$ which can be derived from any system of spatially coupled oscillators in the long-wave limit. The same analysis can be applied to the Wilson-Cowan system [10], but to get the coefficients $b, c > 0$ requires lateral inhibition. Since the Kurmoto result is a long-wave instability, we believe the mechanism in these papers is different from ours which is a finite wavelength instability.

As seen in Figures 2(c) and 9, the pattern formation arises via a period doubling bifurcation of the spatially

homogeneous oscillatory state. In this sense, it is quite reminiscent of bifurcations seen in uniformly periodically forced systems. Crawford [11] and Silber [12] studied these phenomena using symmetry and bifurcation methods and [11] derived a normal form for this bifurcation. However, their set-up was more abstract, so it is unclear whether or not they needed lateral inhibition to obtain the pattern forming states. In a more closely related paper, Rule et al. [13] study the Wilson Cowan equations with uniform periodic driving and found pattern formation both through period doubling and a pitchfork bifurcation. In this paper, they required lateral inhibition. Yang et al. [14] were among the first (to our knowledge) to use Floquet theory to analyze pattern formation in either an intrinsically oscillatory or a periodically forced chemical system. The authors found a variety of patterns arising from a period-doubling bifurcation much as we have seen here. However, they require lateral inhibition in their model.

More recently, [15] studied general two-variable reaction diffusion equations when there was a bulk oscillation. They provide some approximations for conditions on spatial patterns, but once again, the authors require lateral inhibition. Another paper worth mentioning is [16], in which Steyn-Ross et al. consider a mean field model of cortex with inhibitory diffusive coupling to study interneuronal gap junctions. They show that for large values of the inhibitory diffusion constant, D_i, Turing patterns can emerge, while for smaller values of D_i, the homogeneous fixed point can pass through a Hopf bifurcation to give rise to a bulk oscillation. Then, by tuning the inhibitory rate and diffusion constants, so that the system is near a codimension 2 Turing-Hopf bifurcation, they show complex spatiotemporal patterns. Though this seems like a similar setup as ours, the symmetry-breaking mechanism is different: While they analyze perturbations from a homogeneous fixed point and find patterns arising from competing Turing and Hopf instabilities, we linearize around a homogeneous oscillation and show patterns arising from a period-doubling bifurcation. Moreover, they take the diffusion constant of inhibition to be much greater than that of excitation, and thus, keeping with the theme, they require lateral inhibition. Whether or not other systems such as these reaction diffusion systems can show the same types of bifurcations in the absence of lateral inhibition remains an open question.

IX. APPENDIX

1. Linear Stability from a spatially homogeneous Equilibrium

Here we show how to find parameters to obtain pattern formation when $\sigma_e > \sigma_i$ in the WC network with spatial coupling, when considering perturbations from a spatially uniform equilibrium. We make a change of variables to make it easier to explicitly find parameters and consider:

$$u_t = -u + g_e(a_{ee}K_e(x) \star u - a_{ei}K_i(x) \star v)$$
$$\tau v_t = -v + g_i(a_{ie}K_e(x) \star u - a_{ii}K_i(x) \star v)\,,$$

where $g_\mu(J) = (f(J-\theta_\mu) - f(-\theta_\mu))/f'(-\theta_\mu)$ for $\mu = e, i$. (We can readily change to the usual WC equations with a linear change of variables.) This convenient transformation assures that $g_\mu(0) = 0$ and $g'_\mu(0) = 1$. As usual, we suppose that $K_\mu(x) = K(x/\sigma_\mu)/\sigma_\mu$ so that the shapes of the interaction kernels are the same up to a space constant. Let $H_\mu(\omega)$ be the Fourier transform of the kernels, which are normalized so that $H_\mu(0) = 1$. If $\sigma_e < \sigma_i$, then $H_e(\omega) \geq H_i(\omega)$ with equality only at $\omega = 0$. When we linearize around the homogeneous state $(0, 0)$ and take the Fourier transform we see that the resulting matrix (parameterized by ω) has a determinant proportional to

$$D(\omega) = 1 + a_{ii}H_i(\omega) + (a_{ei}a_{ie} - a_{ii}a_{ee})H_e(\omega)H_i(\omega) - a_{ee}H_e(\omega)\,. \quad (5)$$

We want the determinant to be positive for ω near zero and then to become negative for some interval of ω bounded away from 0. We also require that the trace be negative, but since the trace is $-1 + a_{ee}H_e(\omega) - (1 + a_{ii}H_i(\omega))/\tau$, we can always choose τ small enough to ensure that this is negative for all ω. Strictly speaking, we require only that $D(0) > 0$, but in practice, it is generally true that $Q := a_{ei}a_{ie} - a_{ee}a_{ii}$ is also positive. Note that for any reasonable kernels, $H_e(\omega) \to 0$ as $\omega \to \infty$ so that $D(\omega) > 0$ for ω large. We can write the determinant as

$$D(\omega) = 1 + (a_{ii} + QH_e(\omega))H_i(\omega) - a_{ee}H_e(\omega)\,,$$

which makes it clear that decreasing σ_i (increasing $H_i(\omega)$) always makes the determinant more positive and thus pulls the system away from pattern forming instabilities.

2. Conditions on Parameters for Pattern Formation without Lateral Inhibition

Now we want $D(\omega)$ to have a negative minimum value at some value of ω while staying positive when $\omega = 0$. To obtain pattern formation without lateral inhibition, we will set $\sigma_e = \sigma_i$ and then if $D(\omega)$ falls below zero, by continuity, we can choose $\sigma_i < \sigma_e$ so that $D(\omega) < 0$. Now let $w = H_e(\omega) = H_i(\omega)$ and $b = a_{ee} - a_{ii}$ so that $D(\omega) = 1 - bw + Qw^2$. We require that this quadratic have a local minimum at some value of $w \in (0, 1)$. Then the extremum is $w_{min} = b/(2Q)$, and this is a minimum only if $Q > 0$, as we assumed. Then we must have $Q > b/2$, since $w_{min} \in (0, 1)$. Evaluating $D(\omega)$ at the minimum, we have

$$D(\omega_{min}) = 1 - b^2/(2Q) + b^2/(4Q) = 1 - b^2/(4Q)\,.$$

Since this must be negative and $D(1) = 1 - b + Q > 0$, we obtain 3 constraints: (1) $Q > b - 1$, (2) $Q > b/2$, and

(3) $Q < b^2/4$, where only (1) and (3) matter. That is, we need

$$b - 1 < Q < b^2/4\,. \tag{6}$$

If we choose parameters so that (6) is satisfied, then we should be able to obtain pattern formation when $\sigma_i = \sigma_e$. So by continuity, we can find parameters for pattern formation from a spatially homogeneous equilibrium point when σ_i is slightly less than σ_e. Note that this is all in the linearized regime, and so, we must be careful that the nonlinearities do not prove to be an issue (e.g. we get subcritical bifurcations or other homogeneous equilibria).

3. No spread of Inhibition

We close with a remark that with *no spread* of inhibition, there can be no pattern forming instability from a homogeneous equilibrium for then equation (5) becomes:

$$D(\omega) = 1 + a_{ii} + (a_{ei}a_{ie} - a_{ii}a_{ee} - a_{ee})H_e(\omega).$$

This is monotonic in ω so there can be no value of $\omega > 0$ where $D(0) > 0$ and $D(\omega) < 0$.

ACKNOWLEDGMENTS

BE and JH were partially supported by NSF DMS 1219753 and RA was funded through the Undergraduate Program in Neural Computation.

[1] M. C. Cross and P. C. Hohenberg, Reviews of modern physics **65**, 851 (1993).
[2] R. B. Hoyle, *Pattern formation: an introduction to methods* (Cambridge University Press, 2006).
[3] M. Silber and E. Knobloch, Nonlinearity **4**, 1063 (1991).
[4] R. B. Levy and A. D. Reyes, The Journal of Neuroscience **32**, 5609 (2012).
[5] H. Ozeki, I. M. Finn, E. S. Schaffer, K. D. Miller, and D. Ferster, Neuron **62**, 578 (2009).
[6] G. B. Ermentrout and J. D. Cowan, Biological cybernetics **34**, 137 (1979).
[7] J. D. Murray, *Mathematical Biology. II Spatial Models and Biomedical Applications* {*Interdisciplinary Applied Mathematics V. 18*} (Springer-Verlag New York Incorporated, 2001).
[8] "See the supplemental material at [url inserted by publisher] for details regarding the 2d movies that correspond to fig. 8(a)-(c).".
[9] Y. Kuramoto, Progress of Theoretical Physics Supplement **64**, 346 (1978).
[10] G. Ermentrout, in *Competition and cooperation in neural nets* (Springer, 1982) pp. 57–70.
[11] J. D. Crawford, Physica D: Nonlinear Phenomena **52**, 429 (1991).
[12] M. Silber, C. M. Topaz, and A. C. Skeldon, Physica D: nonlinear phenomena **143**, 205 (2000).
[13] M. Rule, M. Stoffregen, and B. Ermentrout, PLoS Comput. Biol **7**, e1002 (2011).
[14] L. Yang, A. M. Zhabotinsky, and I. R. Epstein, Physical review letters **92**, 198303 (2004).
[15] J. D. Challenger, R. Burioni, and D. Fanelli, Physical Review E **92**, 022818 (2015).
[16] M. L. Steyn-Ross, D. A. Steyn-Ross, and J. W. Sleigh, Physical Review X **3**, 021005 (2013).